Metabolic regulation adapting to high methanol environment in the methylotrophic yeast *Ogataea methanolica*

Hao-Liang Cai,[1] Ryohei Doi,[2] Masaya Shimada,[1,2,3]
Takashi Hayakawa[1,2,3] and
Tomoyuki Nakagawa[1,2,3]* iD
[1] The United Graduate School of Agricultural Science, Gifu University, 1-1 Yanagido, Gifu, 501-1193, Japan.
[2] The Graduate School of Natural Sciences and Technologies, 1-1 Yanagido, Gifu, 501-1193, Japan.
[3] The Faculty of Applied Biological Sciences, 1-1 Yanagido, Gifu, 501-1193, Japan.

Summary

Since methylotrophic yeasts such as *Ogataea methanolica* can use methanol as a sole carbon feedstock, they could be applied to produce valuable products from methanol, a next-generation energy source synthesized from natural gases, using genetic engineering tools. In this study, metabolite profiling of *O. methanolica* was conducted under glucose (Glc) and low and high methanol (L- and H-MeOH) conditions to show the adaptation mechanism to a H-MeOH environment. The yeast strain responded not only to the presence of methanol but also to its concentration based on the growth condition. Under H-MeOH conditions, *O. methanolica* downregulated the methanol utilization, glycolytic pathway and alcohol oxidase (AOD) isozymes and dihydroxyacetone synthase (DAS) expression compared with L-MeOH-grown cells. However, levels of energy carriers, such as ATP, were maintained to support cell survival. In H-MeOH-grown cells, reactive oxygen species (ROS) levels were significantly elevated. Along with increasing ROS levels, ROS scavenging system expression was significantly increased in H-MeOH-grown cells. Thus, we concluded that formaldehyde and H_2O_2, which are products of methanol oxidation by AOD isozymes in the peroxisome, are overproduced in H-MeOH-grown cells, and excessive ROS derived from these cells is generated in the cytosol, resulting in upregulation of the antioxidant system and downregulation of the methanol-utilizing pathway to suppress overproduction of toxic intermediates.

Introduction

Given the growing population worldwide and the fact that traditional energy sources such as coal and petroleum that are available for use in industry and daily life are becoming stretched (Xu and Bell, 2014), there is an interest in trying to obtain new energy compounds using other means such as biological conversion. Reduced C_1-compound methanol derived from greenhouse gases and industrial by-products can serve as an inexpensive and clean feedstock for sustainable production of biofuels and commodity chemicals, and it is recognized as one of the next-generation energy sources with the least environmental impact (Whitaker *et al.*, 2015; Antoniewicz, 2019). In this context, biomass conversion (i.e. organic acid, terpenoids and polyketides) of methanol under economic operation has gained much attention over the past two decades (Fei *et al.*, 2014). Methylotrophs provide hosts that are well adapted to specific ecological niches that can use methanol or alternative C_1 feedstocks (Chistoserdova, 2015), and their cell functions have been used in the production of various valuable chemicals (Zhang *et al.*, 2019).

Generally, methylotrophs can be divided into two groups, methylotrophic bacteria and yeasts. Among them, methylotrophic yeasts, such as *Komagataella phaffii* (formerly *Pichia pastoris* [Kurtzman, 2005]), *Candida boidinii*, *Ogataea polymorpha* (formerly *Hansenula polymorpha* [Yamada *et al.,* 1994]), and *Ogataea methanolica* (formerly *Pichia methanolica* [Kurtzman and Robnett, 1998]), have high potential as fermentation producers for several biomass conversions from methanol. They are recognized as attractive hosts for the production of heterologous protein for the following reasons: (i) the yeast is easy to grow to a high-density culture; (ii) abundant molecular genetic tools are available; (iii) the yeast has strong methanol-inducible promoters for the gene expression system; (iv) the yeast has the

advantages of performing extensive post-translational modifications, protein folding and secretion of recombinant targets; and (v) the yeast possesses higher tolerance to extreme (acidic and basic) pH conditions (Porro *et al.*, 2005; Cos *et al.*, 2006; Yurimoto *et al.*, 2011; Palma *et al.*, 2018; Tan *et al.*, 2018; Patiño *et al.*, 2019; Fabarius *et al.*, 2021).

In the methanol-utilizing pathway in methylotrophic yeasts (Fig. 1), methanol is initially oxidized by alcohol oxidase (AOD) to formaldehyde. The generated formaldehyde stands at the branchpoint of the methanol-utilizing pathway between the assimilatory and oxidation pathways. In the assimilatory pathway, formaldehyde is fixed to **D**-xylulose 5-phosphate (Xu5P) by dihydroxyacetone synthase (DAS), generating dihydroxyacetone (DHA) and glyceraldehyde 3-phosphate (GAP). The products continue to be assimilated to form Xu5P, a formaldehyde acceptor, and cell constituents (Sakai *et al.*, 1998; Hartner and Glieder, 2006). The main methanol metabolic process, such as formaldehyde synthesis, formaldehyde fixation and the Xu5P rearrangement pathway, is localized in peroxisomes, which are largely developed up to approximately 80% of the cellular volume in methanol-grown cells (Rußmayer *et al.*, 2015; Fukuoka *et al.*, 2019), while the methanol oxidation pathway containing oxidized nicotinamide adenine dinucleotide (NAD^+)-linked glutathione (GSH)-dependent formaldehyde dehydrogenase (FLD), *S*-formylglutathione hydrolase (FGH) and NAD^+-linked formate dehydrogenase (FDH) occurs in the cytosol (Yurimoto *et al.*, 2011).

Therefore, peroxisomes, which are methanol-inducible microbodies, are the most important organelles in the methylotrophic lifestyle of yeast.

Although features of methylotrophic yeast have a lot in common, some distinctive differences were revealed in *O. methanolica* with species such as *Candida pignaliae* and *C. sonorensis* (Ito *et al.*, 2007). These species possess nine AOD isozymes with different affinities towards methanol and oxygen, which are octamers randomly assembled by two subunits, Mod1p and Mod2p (Nakagawa *et al.*, 1996, 1999, 2001; Fujimura *et al.*, 2007). Specifically, in *O. methanolica*, the *MOD2* gene tends to be expressed at a higher methanol condition than *MOD1*, making it possible to adapt to the concomitantly changing methanol concentrations (Nakagawa *et al.*, 2006). Additionally, the intracellular formaldehyde level was shown to be coordinated by regulating the enzyme expression order; FLD and FDH were induced earlier than AOD isozymes to avoid formaldehyde accumulation in *O. methanolica* (Wakayama *et al.*, 2016). For heterologous protein expression, *O. methanolica* shows better performance than *K. phaffii* in terms of carbon use and gene recombination. The yeast can rapidly adapt its carbon source to shift from glucose to methanol without medium replacement and followed by biomass production (Raymond *et al.*, 1998). Furthermore, *O. methanolica* has two strong AOD promoters (Nakagawa *et al.*, 2006, 2015), and the non-homologous recombination for the expression cassettes performs effectively in *O. methanolica* (Hiep *et al.*, 1993).
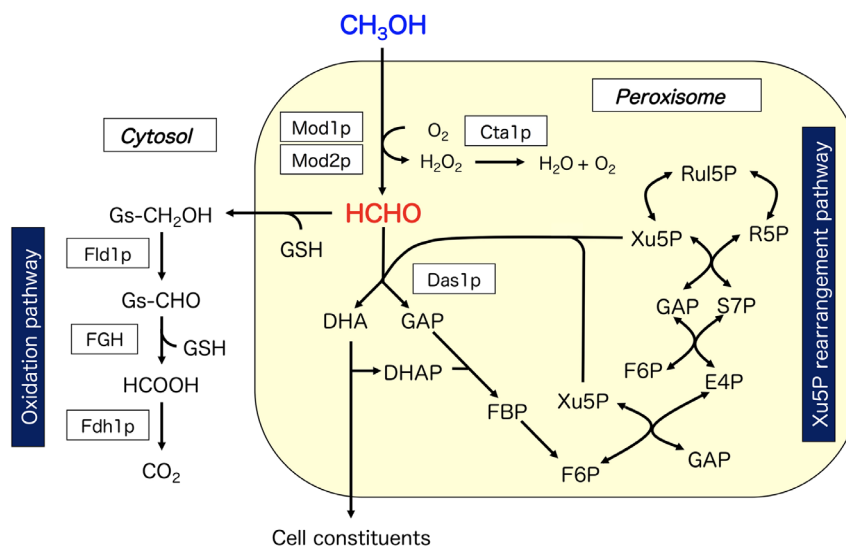

Fig. 1. The methanol metabolic pathway in *O. methanolica*. Mod1p and Mod2p, alcohol oxidase isozymes; Das1p, dihydroxyacetone synthase; Cta1p, catalase; Fld1p, formaldehyde dehydrogenase; FGH, *S*-formylglutathione hydrolase; Fdh1p, formate dehydrogenase; HCHO, formaldehyde; GSH, glutathione; Gs-CH$_2$OH, *S*-hydroxymethylglutathione; Gs-CHO, *S*-formylglutathione; Xu5P, xylulose 5-phosphate; DHA, dihydroxyacetone; GAP, glyceraldehyde 3-phosphate; FBP, fructose 1,6-bisphosphate; F6P fructose 6-bisphosphate; E4P, erythrose 4-phosphate; S7P, sedoheptulose 7-phosphate; R5P, ribose 5-phosphate; Rul5P, ribulose 5-phosphate.
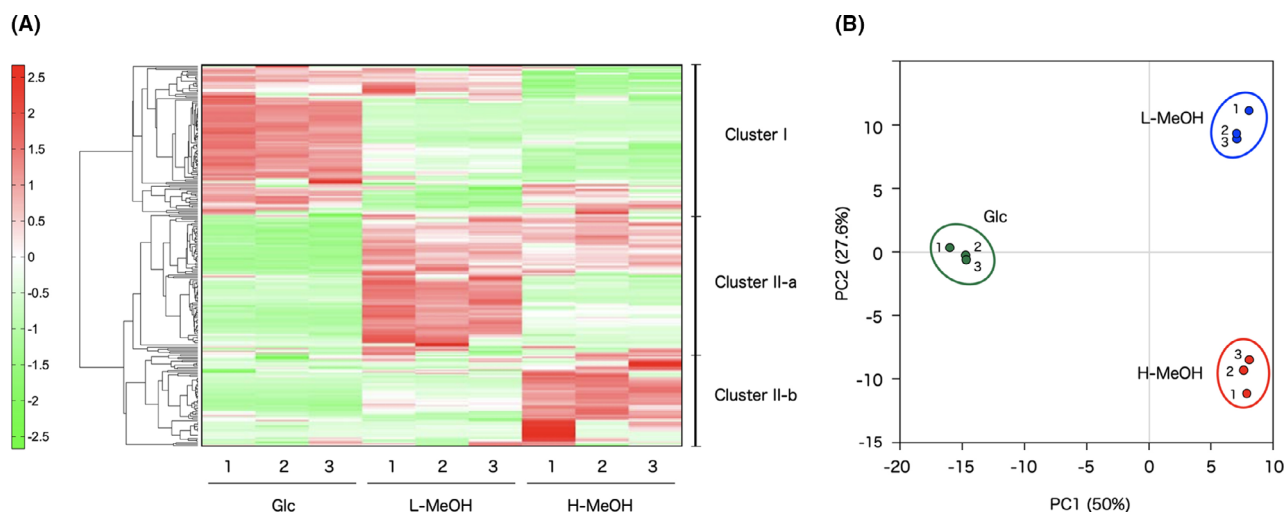
(A)

(B)

Fig. 2. The metabolomic profiles of the intracellular metabolites among *O. methanolica* cells grown in Glc, L-MeOH, and H-MeOH.
A. HCA showed metabolite patterns. Redness and greenness indicate high and low concentration of each metabolite respectively.
B. PCA of the profiling data. Contribution rates are 50.0% for PC1 and 27.6% for PC2. Glc, glucose; L-MeOH, 1% (low) methanol; H-MeOH, 5% (high) methanol; HCA, hierarchical clustering analysis; PCA, principal component analysis.

However, to realize highly productive methanol biomass conversions, a fermentation system that can work efficiently under high methanol conditions, particularly to produce commodity chemicals, is required. Thus, breeding a methylotrophic yeast that grows robustly under high methanol conditions is of great significance. However, all other methylotrophic yeasts including *O. methanolica* exhibit growth inhibition under high methanol conditions, such as over 5%, due to the high intracellular formaldehyde levels, which are extremely toxic to cells (Wakayama *et al.*, 2016). Therefore, to achieve the targeted goal, it is necessary to identify the detailed adaptation mechanism of the yeast to high methanol conditions, and effective countermeasures can then be taken to address the issue.

In this study, to show the adaptation mechanism to high methanol conditions in *O. methanolica,* we aimed to comprehensively investigate the metabolite profiles of *O. methanolica* that were cultivated under low and high methanol conditions and in a glucose medium, together with the expression levels of several key genes that are related to methanol metabolism and the antioxidant system. Our results revealed the molecular mechanism of the *O. methanolica* adaptation to high methanol

conditions and provided useful insights into promoting yeast viability.

Results

Overview of the *O. methanolica* metabolic response to methanol

A previous study showed that *O. methanolica* could grow well below the 3% methanol condition, whereas obvious growth retardation was observed in the 5% methanol condition (Wakayama *et al.,* 2016). In this work, we defined the 1% and 5% methanol conditions as the low methanol condition (L-MeOH) and the high methanol condition (L-MeOH), respectively, and performed metabolomic profiling of *O. methanolica* grown on 1% glucose (Glc), L-MeOH and H-MeOH/YNB media. Overall, there were 259 metabolites (133 cationic and 126 anionic) that were detected overall in the samples (Tables S1 and S2). Hierarchical clustering analysis (HCA) and principal component analysis (PCA) that showed the metabolite patterns are shown in Fig. 2 and Table S3.

HCA-detected metabolites were divided into two large clusters, cluster I and cluster II (Fig. 2A). Cluster I consisted of metabolites that showed a high concentration in

Fig. 3. Metabolic changes among *O. methanolica* cells grown in Glc, L-MeOH and H-MeOH. (A) Intermediates in the methanol-utilizing pathway, glycolysis and TCA cycle; (B) vitamin B complex; and (C) energy carriers. Results are shown as the mean and standard deviation ($n = 3$). *Significantly different between each group at $P < 0.05$ as determined by Student's *t*-test. Glc, glucose; L-MeOH, 1% (low) methanol; H-MeOH, 5% (high) methanol; TCA, tricarboxylic acid cycle; DHA, dihydroxyacetone; DHAP, dihydroxyacetone phosphate; E4P, erythrose 4-phosphate; FBP, fructose 1,6-bisphosphate; F6P, fructose 6-phosphate; FAD, flavin adenine dinucleotide; FMN, flavin mononucleotide; GAP, glyceraldehyde 3-phosphate; NA, nicotinamide; PA, pantothenic acid; PM, pyridoxamine; PMP, pyridoxamine 5′-phosphate; R5P, ribose 5-phosphate; Rul5P, ribulose 5-phosphate; RF, riboflavin; S7P, sedoheptulose 7-phosphate; Thi, thiamine; TPP, thiamine pyrophosphate; Xu5P, xylulose 5-phosphate.
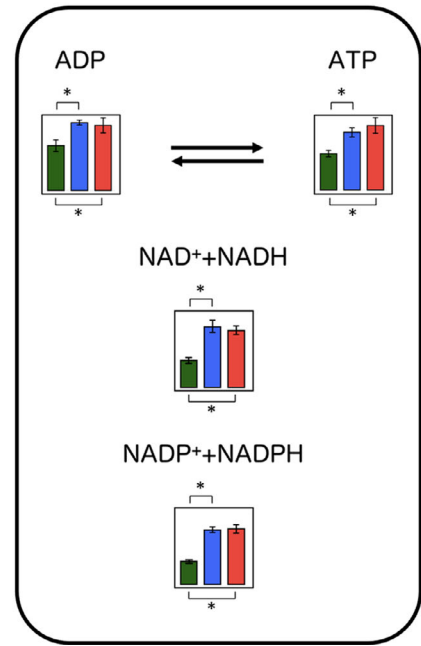
(A) Methanol metabolism
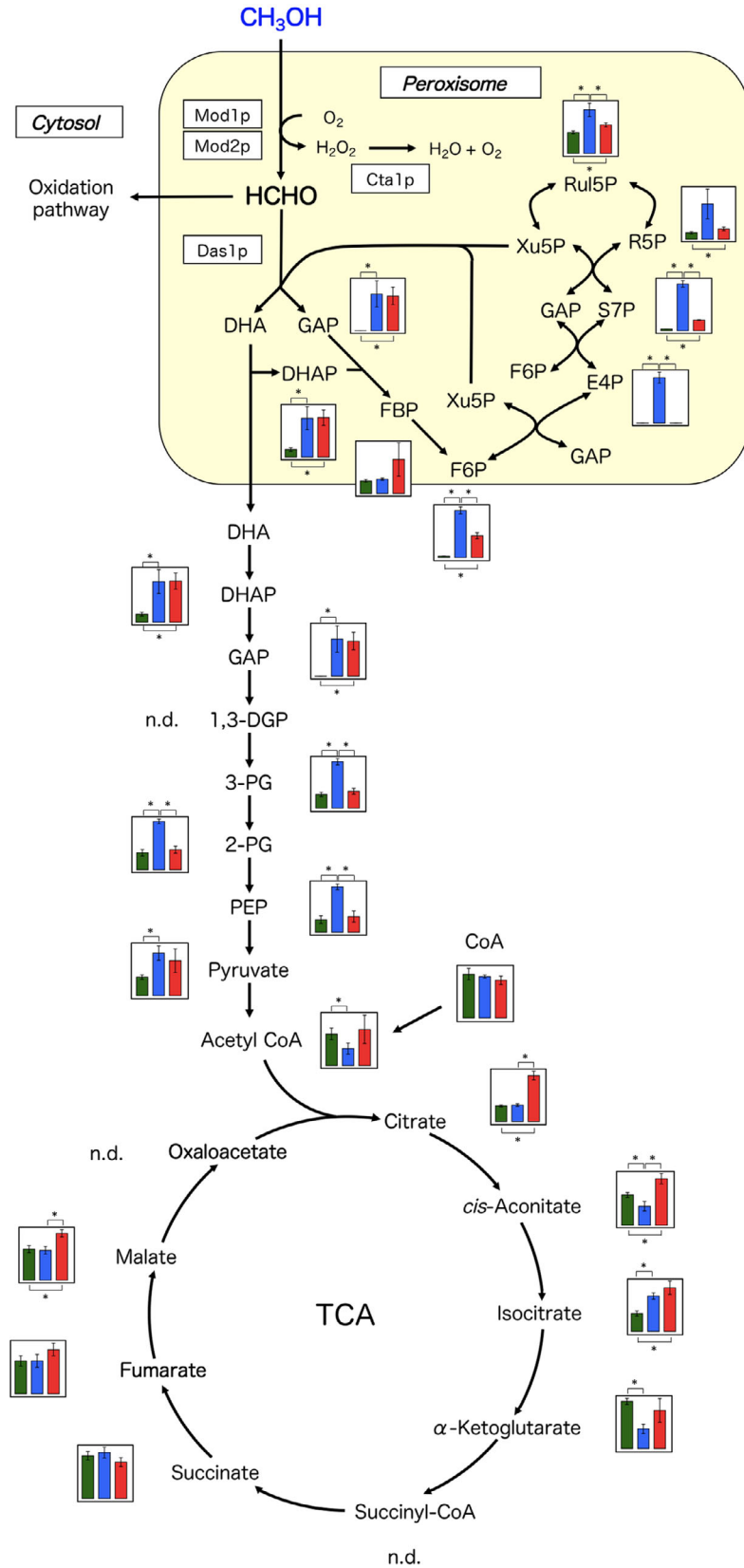
(B) Vitamin B complex
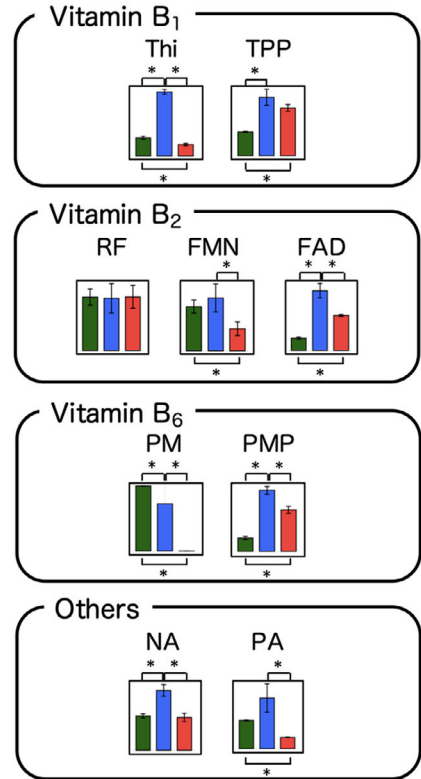
(C) Energy carriers

Glc-grown cells, and cluster II contained metabolites that had a high concentration in MeOH-grown cells. Moreover, cluster II included two subclusters; i.e., cluster II-a contained metabolites with a high concentration in L-MeOH-grown cells, and cluster II-b consisted of metabolites with a high concentration in H-MeOH-grown cells (Fig. 2A).

According to the PCA results, the cumulative variation proportions of the first two principal components were 50.0% and 77.6%. PC1 completely separated Glc-grown cells and MeOH-grown cells with a proportion of 50.0%, indicating that Glc- and MeOH-grown cells have specific metabolomic compounds compared with each other and that *O. methanolica* alters its metabolome to adapt to MeOH growth conditions (Fig. 2B). However, a metabolic change also occurred between L- and H-MeOH-grown cells, as shown in the PCA plot (Fig. 2B). PC2 completely segregated L-MeOH and H-MeOH, showing significantly different metabolite contents at different methanol concentrations ($P < 0.05$).

These results indicate that *O. methanolica* responds to the presence of methanol and to its concentration in the growth condition and that the yeast coordinates the methanol metabolism based on the MeOH concentration in the growth condition.

Metabolomic profiles of methanol-utilizing pathways in L-MeOH-grown cells

Initially, we compared the change in the metabolite levels involved in the main methanol-utilizing pathway between Glc- and L-MeOH-grown cells (Fig. 3A). In L-MeOH-grown cells, most of the metabolite levels that are involved in the Xu5P rearrangement pathway and glycolysis were largely increased compared with Glc-grown cells, except for acetyl coenzyme A (CoA) and fructose 1,6-bisphosphate (FBA). Because Xu5P is an epimer of Rul5P, neither metabolite could be distinguished from each other in this analysis. Thus, we could not show individual Xu5P metabolite levels in this study, but the complex Xu5P/Rul5P metabolite level was significantly increased in L-MeOH-grown cells. Most intermediates in the peroxisomal Xu5p rearrangement pathway are also those of the pentose phosphate pathway in the cytosol that could not be distinguished by this method. However, a significant increase in these metabolites in L-MeOH-proliferating cells indicates activation of methanol assimilation in the peroxisome compartment.

Expression of *MOD1*, *MOD2* and *DAS1*, which encode AOD isozymes and DAS, was strongly upregulated in L-MeOH-grown cells and completely repressed in Glc-grown cells (Fig. 4A). Expression of *FLD1* and *FDH1*, which encode FLD and FDH, was also strongly upregulated in L-MeOH conditions (Fig. 4A). These results are

consistent with those of previous reports (Nakagawa *et al.*, 2004, 2010a, 2015). Moreover, intracellular levels of thiamine pyrophosphate (TPP) and flavin adenine dinucleotide (FAD), which are co-enzymes for AOD isozymes and DAS, respectively, in L-MeOH-grown cells were significantly increased compared with Glc-grown cells ($P < 0.05$; Fig. 3B).

Levels of most metabolites that are involved in glycolysis, such as 3-phosphoglycerate (3-PG), 2-phosphoglycerate (2-PG), phosphoenolpyruvate (PEP) and pyruvate, were significantly increased compared with those of Glc-grown cells, although intracellular levels of acetyl-CoA and several TCA cycle metabolites were decreased (Fig. 3A).

These results are comparable to previous reports on methanol induction of methanol metabolic pathways in other methylotrophic yeast strains (Rußmayer *et al.*, 2015), indicating that *O. methanolica* upregulates the methanol-utilizing pathway, including glycolysis and the Xu5P rearrangement pathway, under L-MeOH conditions.

Metabolomic profiles of the methanol-utilizing pathways in H-MeOH-grown cells

In H-MeOH-grown cells, the levels of most metabolites that are involved in the Xu5P rearrangement pathway were also significantly reduced compared with L-MeOH-grown cells, and their levels were similar to those in Glc-grown cells (Fig. 3A). In particular, erythrose 4-phosphate (E4P) in the Xu5P rearrangement pathway was rarely detected, and Xu5P (Rul5P), fructose 6-phosphate (F6P), sedoheptulose 7-phosphate (S7P) and ribose 5-phosphate (R5P) levels were significantly decreased ($P < 0.05$). Moreover, the metabolite levels involved in glycolytic pathways, such as 3-PG, 2-PG and PEP, were also significantly reduced compared with L-MeOH-grown cells, although TCA cycle and acetyl-CoA metabolite levels were increased (Fig. 3A).

In H-MeOH-grown cells, *MOD2* and *FDH1* expression was significantly downregulated compared with that in L-MeOH-grown cells, and *MOD1* and *DAS1* expression tended to decrease (not significantly). However, *FLD1* was strongly expressed in H-MeOH-grown cells with no significant difference compared with L-MeOH-grown cells (Fig. 4A). AOD activity was suppressed in H-MeOH-grown cells (Fig. 4B). Thus, *O. methanolica* may downregulate methanol metabolism on purpose under H-MeOH conditions.

In H-MeOH-grown cells, intracellular levels of most vitamin B complex members significantly decreased compared with L-MeOH-grown cells, except for TPP ($P < 0.05$; Fig. 3B). The nicotinamide (NA) level also decreased in H-MeOH-grown cells, but intracellular
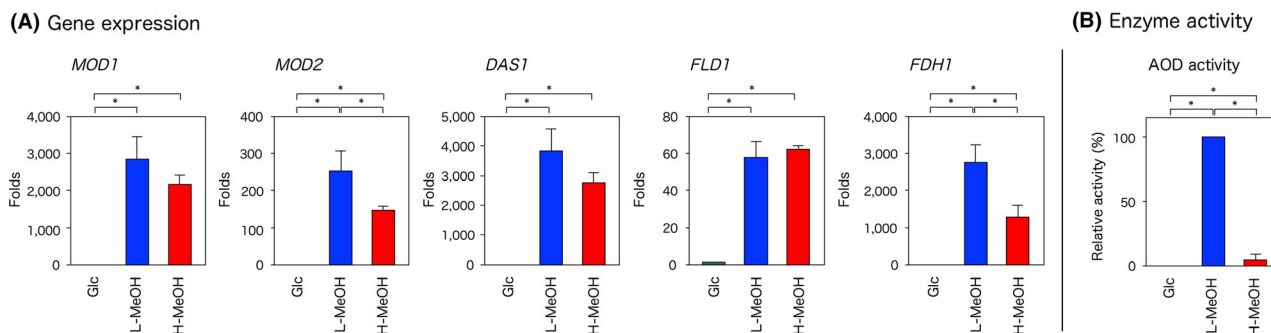
(A) Gene expression

(B) Enzyme activity

Fig. 4. The gene expression of methanol-utilizing enzymes and methanol oxidation pathway (A) and induction of AOD activity (B). Data represent the mean $\pm$ SD ($n = 3$). Statistical differences between Glc-, L-MeOH- and H-MeOH-grown cells were determined. *Significantly different between each group at $P < 0.05$ as determined by the Student's t-test. AOD, alcohol oxidase; SD, standard deviation; Glc, glucose; L-MeOH, 1% (low) methanol; H-MeOH, 5% (high) methanol.

nicotinamide adenine dinucleotide phosphate (NADP$^+$) levels did not change. Because formaldehyde-metabolizing enzymes, such as DAS, FLD and FDH, require TPP and NAD$^+$ for their activity, H-MeOH-grown cells seem to regulate their levels to avoid intracellular formaldehyde accumulation. Levels of pantothenic acid (PA), the precursor of CoA, were also decreased, but the amount of CoA did not change between L- and H-MeOH-grown cells. In contrast, intracellular levels of aminosugars, such as N-acetylglucosamine (GlcNAc), N-acetylglucosamine 1-phosphate (GlcNAc-P) and N-acetylglucosamine 6-phosphate (NAcGlcNP), increased in H-MeOH-grown cells compared with Glc- and L-MeOH-grown cells (Table S2).

This indicates that *O. methanolica* regulates the methanol-utilizing pathway to repress expression of specific enzymes for methanol metabolism, followed by production of the intermediates in the Xu5P rearrangement pathway. The glycolytic pathway was then down-regulated in H-MeOH-grown cells, while other pathways might be upregulated to supply acetyl-CoA that led to the elevated TCA cycle metabolites.

Cells can maintain the intracellular energy levels regardless of the methanol condition

For energy carriers, we observed intracellular ATP/ADP, NADH+NAD$^+$ and NADPH+NADP$^+$ levels in Glc-, L-MeOH- and H-MeOH-grown cells (Fig. 3C). Intracellular ATP, NADH+NAD$^+$ and NAD PH+NADP$^+$ levels in L-MeOH-grown cells were significantly higher than those in Glc-grown cells. However, intracellular ATP, NADH+-NAD$^+$ and NADPH+NADP$^+$ levels did not fluctuate between L-MeOH- and H-MeOH-grown cells ($P < 0.05$; Fig. 3C). These results indicate that *O. methanolica* well coordinates the methanol-utilizing pathway to maintain constant energy levels in the cell under any methanol condition.

Cells enhance the ROS scavenging system under H-MeOH conditions

In the methanol metabolic pathway, GSH has important physiological roles, such as an acceptor of formaldehyde in the methanol oxidation pathway (Fig. 5A) and an electron donor for glutathione peroxidase (Gpx1p) and peroxisomal peroxiredoxin (Pmp20) (Fig. 5B) (Horiguchi *et al.*, 2001a; Yano *et al.*, 2009). Thus, intracellular GSH and oxidized glutathione (GSSG) levels are

(A) MeOH oxidation pathway　　**(B)** ROS scavenging pathway
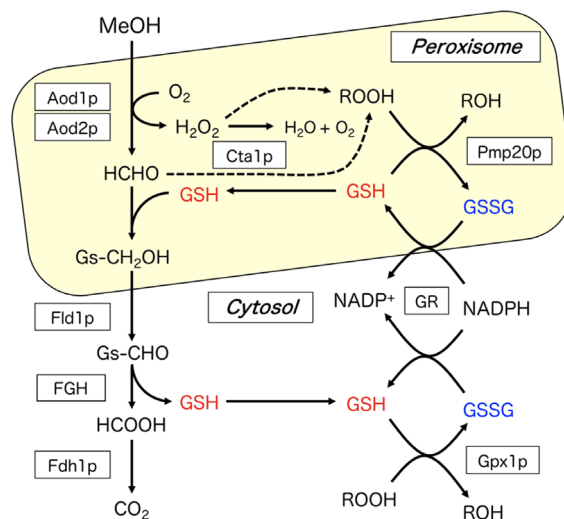
Fig. 5. The glutathione redox system and its related metabolism. (A) Methanol oxidation and (B) ROS scavenging pathways. Dashed arrow, hydroxyl radicals from H_2O_2 attack membranes that result in the generation of ROOH (Horiguchi *et al.*, 2001a). Cta1p, catalase; Fld1p, formaldehyde dehydrogenase; FGH, S-formylglutathione hydrolase; Fdh1p, formate dehydrogenase; Pmp20, peroxisomal glutathione peroxidase; Gpx1p, glutathione peroxidase; Gs-CH$_2$OH, S-hydroxymethyl glutathione; Gs-CHO, S-formylglutathione; GSH, reduced glutathione; GSSG, oxidized glutathione; ROS, reactive oxygen species; ROOH (where R is an aliphatic or aromatic organic group or simply hydrogen), alkyl hydroperoxide.

(A) GSH and GSSG

(B) ROS and TBARS

Fig. 6. GSH and GSSG (A) and ROS and TBARS (B) levels in Glc, L-MeOH, and H-MeOH-grown *O. methanolica*. Data represent the mean $\pm$ SD (n = 3). Statistical differences between Glc-, L-MeOH- and H-MeOH-grown cel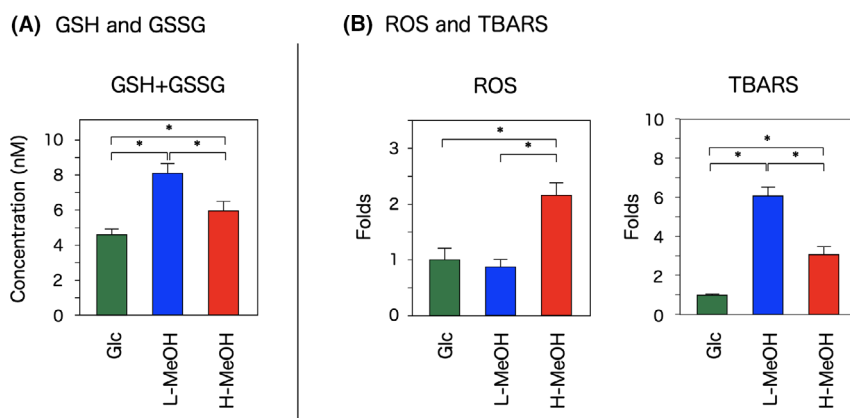ls were determined. *Significantly different between each group at P < 0.05 as determined by Student's t-test. GSH, glutathione; GSSG, oxidized glutathione; Glc, glucose; L-MeOH, 1% (low) methanol; H-MeOH, 5% (high) methanol; SD, standard deviation.

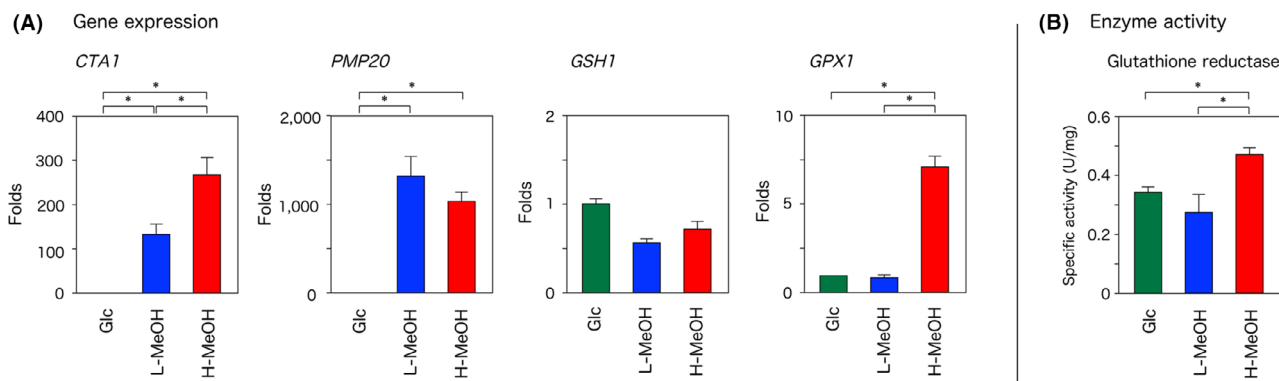**(A)** Gene expression

(B) Enzyme activity

Fig. 7. The gene expression (A) and induction (B) of the enzymes participating the ROS scavenging system in Glc, L-MeOH and H-MeOH-grown *O. methanolica*. Data represent the mean $\pm$ SD (n = 3). Statistical differences between the Glc-, L-MeOH- and H-MeOH-grown cells were determined. *Significantly different between each group at P < 0.05 as determined by the Student's t-test. ROS, reactive oxygen species; Glc, glucose; L-MeOH, 1% (low) methanol; H-MeOH, 5% (high) methanol; SD, standard deviation.

some of the most important factors in methanol metabolism in methylotrophic yeast. Therefore, we observed the intracellular GSH+GSSG level in Glc-, L-MeOH- and H-MeOH-grown cells (Fig. 6A). Intracellular levels of GSH+GSSG were significantly increased in L-MeOH-grown cells compared with Glc-grown cells (P < 0.05). However, in H-MeOH-grown cells, intracellular levels of GSH+GSSG were less than those in L-MeOH-grown cells (P < 0.05). Expression of *GSH1*, which encodes γ-glutamylcysteine synthetase that catalyses the first step of GSH biosynthesis, was not changed among Glc-, L-MeOH- and H-MeOH-grown cells (Fig. 7A), and glutathione reductase (GR) activity, protecting cells from ROS, was induced only in H-MeOH-grown cells (Fig. 7B).

Excessive intracellular ROS, such as superoxide ($O_2^{\bullet-}$) or hydrogen peroxide (H_2O_2), can deplete reducing substrates, ultimately leading to oxidative damage

and cytotoxicity (Rubattu *et al.*, 2014), and thiobarbituric acid reactive substances (TBARS) are one of the main ROS degradation products (Pryor, 1991). Thus, intracellular ROS and TBARS levels were compared among Glc-, L-MeOH- and H-MeOH-grown cells (Fig. 6B). The ROS level was not changed between L-MeOH- and Glc-grown cells, but in H-MeOH-grown cells, it was significantly increased. Intracellular TBARS levels significantly increased in L-MeOH-grown cells, but not in H-MeOH-grown cells, and TBARS reduced to the level similar to that in Glc-grown cells (Fig. 6B).

Expression of *CTA1* encoding peroxisomal/cytosol catalase and *PMP20* encoding peroxisomal peroxiredoxin was upregulated by methanol. *CTA1* and *PMP20* showed strong expression in L-MeOH-grown cells; *CTA1* expression was further upregulated in H-MeOH-grown cells (Fig. 7A). Although *GPX1* expression was not changed between Glc- and L-MeOH-grown cells, its

expression was significantly upregulated in H-MeOH-grown cells (Fig. 7).

These results suggest that *O. methanolica* upregulated its antioxidant system, including Cta1p, Gpx1p and GR, in H-MeOH-grown cells based on excessive ROS accumulation levels, and the GSH/GSSG ratio might be correspondingly increased.

Morphology of peroxisomes in H-MeOH-grown cells

Finally, the morphology of peroxisomes in L- and H-MeOH-grown cells was observed using the GFP-PTS1/WT strain expressing green fluorescent protein (GFP)-tagged peroxisome targeting signal 1 (PTS1) (Fig. 8). In L-MeOH-grown cells, the fluorescence pattern showing the locations of peroxisomes occupied a large part of the cellular volume. This indicated that the peroxisomes underwent strong proliferation in the L-MeOH condition. However, in H-MeOH-grown cells, the peroxisomes also underwent proliferation, but the size of the peroxisome cluster was smaller than that in L-MeOH-grown cells (Fig. 8). This is because the expression of peroxisomal enzymes, such as AODs, DAS and Pmp20, was suppressed in H-MeOH-grown cells (Figs 4A and 7A). The morphological change in peroxisome was stably observed in H-MeOH-grown cells with high reproducibility (Fig. S1).

Discussion

In this study, we aimed to reveal the metabolic aspect of *O. methanolica* in methylotrophic growth, especially under H-MeOH conditions, to learn about the high methanol adaptation system in yeast. Using CE-TOFMS, 92 target metabolites were quantified in the *O. methanolica* cell (Table S3). Because these metabolites covered almost all of the core cell metabolic pathways, such as glycolysis, the TCA cycle and glutathione metabolism, metabolomics data in this research could characterize the dynamic metabolic activities in *O. methanolica* with exposure to different growth environments. Indeed, intracellular metabolite levels in the yeast varied between L- and H-MeOH conditions, providing insights into the

molecular mechanism for adaptation to H-MeOH conditions in methylotrophic yeast. We believe that improving the adaptability of methylotrophic yeasts to the H-MeOH condition could promote their high methanol utilization and heterologous production capabilities for industrial applications.

We first showed regulation of the methanol-utilizing pathway responses to carbon sources and the methanol concentration in *O. methanolica*. In L-MeOH-grown cells, metabolite levels in the Xu5P rearrangement pathway and glycolysis were significantly increased compared with Glc-grown cells, and expression of genes encoding the methanol metabolic enzymes was strongly upregulated. This flux shifting between Glc- and L-MeOH-grown cells was similar to the case of *K. phaffii* (Rußmayer *et al.*, 2015). Because the efficiency of the methanol assimilatory process is dependent on the Xu5P supply rate (Douma *et al.*, 1985), enhancement of the Xu5P rearrangement pathway together with methanol metabolic enzymes during methylotrophic yeast growth is reasonable, and our data indicate that the L-MeOH condition is also suitable for *O. methanolica* methylotrophic growth with a low metabolic burden.

In contrast, in H-MeOH-grown cells, the Xu5P rearrangement pathway and glycolysis were downregulated to the same level compared with Glc-grown cells. Formaldehyde is known to be a highly toxic intermediate in methanol metabolism so yeast must carefully regulate formaldehyde flux over the oxidative and assimilation pathways during methylotrophic growth. For *O. methanolica*, intracellular formaldehyde can also be regulated by AOD isozymes at a constant level under low methanol conditions (Nakagawa *et al.*, 2002). However, AOD isozymes could not regulate the intracellular formaldehyde level in H-MeOH-grown cells, because Mod2p, which is the low-affinity type of AOD subunit for methanol, can fully function as a formaldehyde producer under these conditions, together with Mod1p. Therefore, H-MeOH-grown cells may downregulate AOD activity and all methanol metabolism to avoid excessive formaldehyde accumulation in the cell. Moreover, because excessive formaldehyde produced in peroxisomes leaks into the cytosol, the cell needs to address its toxic effect in the
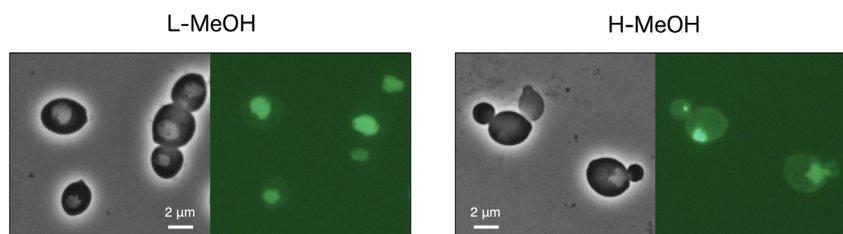
L-MeOH   H-MeOH

Fig. 8. Morphology of peroxisomes in L-MeOH- and H-MeOH-grown cells using strain GFP-PTS1/WT. L-MeOH, 1% (low) methanol; H-MeOH, 5% (high) methanol.

cytosol. Thus, to maintain a functional level of formaldehyde detoxification in the cytosol, *FLD1* expression was not suppressed under H-MeOH conditions, although *FDH1* expression was significantly suppressed (Fig. 3).

Furthermore, GSH is a key factor in methanol metabolism in methylotrophic yeast because FLD catalyses the dehydrogenation of *S*-(hydroxymethyl) GSH, which forms between formaldehyde and GSH via a non-enzymatic reaction. Therefore, *O. methanolica* increases intracellular GSH and GSSG levels during methylotrophic growth. In H-MeOH-grown cells, intracellular GSH+GSSG levels were visibly decreased compared with L-MeOH-grown cells because GSH forms *S*-(hydroxymethyl) GSH with excessively accumulated formaldehyde in the cell. Therefore, *O. methanolica* should promote GR activity in H-MeOH-grown cells to enhance intracellular GSH levels in order to maintain the intracellular level of reductive form, GSH, at a high level.

Additionally, GSH has two important physiological roles as an acceptor of formaldehyde and an antioxidant compound in methylotrophic yeast growth because AOD produces a large amount of H_2O_2 in the peroxisome. The cellular ROS level was also reported to be significantly elevated by the presence of formaldehyde (Cui *et al.*, 2016). In this study, the intracellular ROS level was remarkably increased in H-MeOH-grown cells, while the yeast that was grown under L-MeOH conditions maintained a similar ROS level compared with Glc-grown cells. The intracellular level of lipid oxidation products was also significantly increased in MeOH-grown cells. Gene expression for the antioxidant system in the peroxisome, such as *CTA1* and *PMP20*, was largely expressed under MeOH conditions, but *GPX1* expression encoding cytosolic GSH peroxidase was strongly upregulated only in H-MeOH-grown cells. It was reported that approximately half of the amount of Cta1p in methylotrophic yeast grown on methanol were localized in the cytoplasm together with the peroxisome (Horiguchi *et al.*, 2001b; Nakagawa *et al.*, 2010b). Therefore, *O. methanolica* strongly induces the peroxisomal antioxidant system in the presence of methanol, and it also enhances the cytosolic antioxidant system under H-MeOH conditions. Additionally, under L-MeOH conditions, Cta1p and Pmp20p can control intracellular ROS and lipid peroxide levels in the peroxisome. Cytosolic Cta1p, Gpx1p and GR were also induced by ROS that were derived from excessive formaldehyde that was leaked from the peroxisome in H-MeOH-grown cells, and the cytosolic antioxidant system scavenges ROS including lipid peroxide in the cytosol under high methanol conditions.

Cellular energy is the foundation of good metabolic performance, and energy levels were maintained in *O. methanolica* regardless of the methanol concentration (Fig. 3C). In methanol-grown methylotrophic yeasts, the cellular energy sources are mainly supplied in two ways: (i) TCA cycle reactions through the respiratory chain; and (ii) the methanol utilization pathway for NADH production, which is then transported via the inner mitochondrial membrane for ATP generation. In L-MeOH-grown cells, the overall abundance of intermediates in the TCA cycle was lower than that of the other two conditions, which might be due to the accumulated intermediates level in the glycolytic pathway, but intracellular level of acetyl-CoA was significantly downregulated in L-MeOH-grown cells (Fig. 3A). Rußmayer *et al.* (2015) reported that the TCA cycle flux in *K. phaffii* was downregulated in methanol/glycerol-grown cells and was mainly controlled by the lower influx of acetyl-CoA into the TCA cycle. Therefore, the TCA cycle flux in *O. methanolica* is also downregulated by the intracellular level of acetyl-CoA in L-MeOH-grown cells, as in *K. phaffii*. Meanwhile, in *O. methanolica*, the expression levels of *FLD1* and *FDH1* were enhanced in L-MeOH-grown cells (Fig. 4A). These findings indicate that the methanol oxidation pathway has an important function as an NADH supply in L-MeOH-grown cells, and that the TCA cycle is mainly employed to produce metabolic precursors for biomass formation rather than energy transduction through the respiratory chain.

In contrast, the cellular energy status in H-MeOH-grown cells was well maintained and the ATP level was even higher than that in L-MeOH-grown cells, although methanol metabolism was downregulated (Fig. 3C). This might be attributed to the increased intracellular level of acetyl-CoA in H-MeOH-grown cells, which was approximately twofold higher than that in L-MeOH-grown cells. Correspondingly, the TCA cycle was activated, as reflected by the much higher abundance of intermediates in the H-MeOH condition. We assume that the fatty acid β-oxidation pathway might be utilized as an acetyl-CoA supply system because, in *K. phaffii*, its gene expression was upregulated in H-MeOH-grown cells (unpublished data). Furthermore, the expression level of *FLD1* maintained in the H-MeOH condition is advantageous to the stability of the intracellular levels of NAD(P)H/NAD(P)$^+$ because the methanol oxidation pathway is localized in the cytosol. In this context, it was suggested that methylotrophic yeast might maintain their energy status for cell survival and adaptation by promoting the TCA cycle flux in H-MeOH conditions.

In conclusion, we introduced a metabolomics approach to elucidate the molecular mechanism for adaptation to high methanol conditions in *O. methanolica* from the viewpoint of the metabolome profile. Our results suggest that, under H-MeOH conditions, the methanol-utilizing pathway was severely downregulated to reduce intracellular formaldehyde levels to normal, while the antioxidant system was strongly induced to remove

excessive ROS that were derived from toxic intermediates in methanol metabolism, *i.e.* H_2O_2 and formaldehyde. Through these regulation systems, the cells coordinate all of the metabolic pathways to maintain homeostasis of the intracellular energy state. We also identified several intermediates that showed intracellular levels that significantly increased or decreased in H-MeOH-grown cells, such as amino sugars and some amino acids (Table S3). The functions of these compounds in adaptation to high methanol conditions have not been previously analysed, and we believe that these compounds will provide useful information on the molecular mechanism in methylotrophic yeast *O. methanolica*. Information on the molecular mechanism for adaptation to the H-MeOH condition could be applied to breeding the super C_1 yeast strain of *O. methanolica*. Moreover, a bred yeast strain that is enhanced with H-MeOH tolerance would be advantageous for use in a methanol bioconversion system. Therefore, we believe that the findings obtained in this study will contribute to the construction of an innovative carbon-neutral material circulation system.

Experimental procedures

Yeast strain and culture conditions

O. methanolica IAM 12901 (=CBS 6515=ATCC 58372) and PMAD11 (*ade2-11*) (Raymond *et al*., 1998) (Invitrogen, Carlsbad, CA, USA) that were derived from the type strain were used as the test strains. Strain GFP-PTS1/WT expressing GFP with peroxisome targeting signal 1 (PTS1) at the C-terminus in strain PMAD11 was used to observe peroxisome proliferation (Ito *et al*., 2011).

Complex YPD medium containing 1% (w/v) yeast extract, 2% (w/v) peptone and 2% (w/v) dextrose was used for preculture of *O. methanolica* strains. For induction and growth tests, synthetic YNB medium was used. The carbon source in the YNB medium was one of the following: 1% (v/v) methanol (low methanol condition [L-MeOH]), 5% (v/v) methanol (high methanol condition [H-MeOH]) or 1% (w/v) glucose (control condition [Glc]). For strain PMAD11, 0.01% (w/v) adenine was added into the YNB medium.

The initial pH of the medium was adjusted to 6.0. Cultivation (120 ml) was performed aerobically at 28°C with rotary shaking at 150 rpm in 500-ml Erlenmeyer flasks.

Sample preparation for CE-TOFMS

For the metabolome analysis of the *O. methanolica*, strain IAM 12901 was precultured in the YPD medium. The cells, the OD_{660nm} of which was 1.0, were collected by centrifugation at 10 000 $\times$ *g* for 10 min, and washed three times using sterilized water. Then, cells were transferred to L-MeOH/YNB, H-MeOH/YNB and Glc/YNB media, and the strain was incubated aerobically at 28°C for 8 h in triplicate. Cells were collected by centrifugation at 10,000 $\times$ *g* for 10 min, washed three times using sterilized ultrapure water and then frozen in liquid N_2. Metabolites were extracted using a previously described method (Ohashi *et al*., 2008) with modifications. Approximately 60 mg of cells was suspended in 600 μl of methanol containing 200 μM 1,4-piperazine-diethanesulfonic acid and 200 μM methionine sulfone as internal standards. After fully mixing using an MT-200 microtube mixer (Tomy, Tokyo, Japan) six times for 2 min each at 4°C, the samples were centrifuged at 4°C, 16 000 $\times$ *g* for 5 min. The supernatant (300 μl) was centrifuged through a Millipore 5 kDa cut-off filter (Merck, Billerica, MA, USA) at 10 000 $\times$ *g* for 60 min. The filtrate was vacuum-dried for 2 h, dissolved in Milli-Q water and immediately analysed using CE-TOFMS.

Capillary electrophoresis time-of-flight mass spectrometry (CE-TOFMS) analysis

Metabolome analysis was conducted according to HMT's *Basic Scan* package, using CE-TOFMS based on the methods described previously (Ohashi *et al*., 2008; Ooga *et al*., 2011). Briefly, a fused silica capillary of 80 cm $\times$ 50 μm i.d. was used to analyse cationic and anionic metabolites with run and rinse buffer solutions (p/n: H3301-1001 for the cation and H3302-1021 for the anion [Human Metabolome Technologies, Tsuruoka, Yamagata, Japan]). Sample injection to detect cationic and anionic metabolites was performed at a pressure of 50 mbar for 10 and 25 s, with capillary electrophoresis voltage applied at 27 and 30 kV respectively. Electrospray ionization MS was performed with a capillary electrophoresis voltage that was set to positive and 4 kV and to negative and 3.5 kV for the cationic and anionic mode determination respectively. For stabilization of MS analysis, the sheath solution (p/n: H3301-1020) was supplied by Human Metabolome Technologies. The spectrometer scanned from range of *m/z* 50 to 1000.

Analyses of the metabolite levels

Analyses of the metabolite levels were performed in accordance with the method of Sugimoto *et al*. (2010) using the proprietary software MASTERHANDS (Institute for Advanced Biosciences, Keio University, Japan). HCA was processed using MATLAB 2008a (MathWorks, Natick, MA, USA). PCA was processed using JMP version 9.0.2 (SAS Institute, Cary, NC, USA). Multivariate analyses were performed using IBM SPSS Statistics 21, and data were considered significantly different if $P < 0.05$

(indicated by *) in the analysis of variance (ANOVA). The results were plotted using ORIGIN 9.1. All data are expressed as the mean $\pm$ standard error. Unless specified, all tests were performed in triplicate.

Real-time quantitative polymerase chain reaction (qPCR)

For qPCR, strain IAM 12901 was precultured in the YPD medium and then induced for 2 h in each YNB medium in triplicate. Total RNA was extracted from strain IAM 12901 cells using a Qiagen RNeasy mini kit (Qiagen K.K. Japan, Tokyo, Japan), and cDNA was synthesized with a ReverTra Ace qPCR RT Kit (Toyobo, Osaka, Japan). qPCR was performed in a final volume of 20 µl, which contained SYBR Green, 0.2 µmol l^{-1} of each primer, Rox reference dye and 20 ng of cDNA, using SYBR Premix Ex Taq (Takara Bio, Kusatsu, Japan) and a StepOnePlus Real-Time PCR System (Applied Biosystems Japan, Tokyo, Japan). Primers that were used in this study are listed in Table S4. Each specific relative mRNA expression level was determined based on the $2^{-\Delta\Delta CT}$ method (Livak and Schmittgen, 2001). All gene expression values were normalized using the *URA3* C_T value.

Preparation of cell-free extracts

The cells induced by Glc/YNB, H-MeOH/YNB and H-MeOH/YNB were lysed in five 30-s pulses using a Mini Bead Beater (BioSpec Products, Bartlesville, OK, USA), followed by centrifugation at 16 000 $\times$ *g* for 10 min at 4°C to remove unbroken cells and insoluble cellular debris. The cell-free supernatants were prepared in triplicate and immediately subjected to the ROS and enzyme assays.

Protein concentrations of the cell-free extracts were determined using a Bradford protein assay kit (Bio-Rad Laboratories, Hercules, CA, USA) with bovine serum albumin as the standard (Bradford, 1976).

Measurements of the intracellular oxidized lipid and ROS levels

Intracellular oxidized lipid levels were measured using the TBARS method (Jentzsch *et al.*, 1996). Intracellular ROS levels were measured by the method that was described by Matsufuji *et al.* (2013), using an oxidant-sensitive probe 2,7-dichlorodihydrofluorescein diacetate (DCFDA; Molecular Probes, Eugene, OR, USA). This probe was trapped inside the cells after diacetate cleavage by an intracellular esterase (Royall and Ischiropoulos, 1993) and oxidized by radical species to produce a fluorescent compound that emitted a different wavelength (Tsuchiya *et al.*, 1994).

Glutathione reductase (GR) assay

GR activity was measured according to previously published methods with slight modifications (Grant *et al.*, 1996). One unit for GR activity was defined as the amount of enzyme that was required to catalyse the disappearance of 1 µmol of NADPH per minute under the conditions, as described by Foyer and Halliwell (1976).

Fluorescence microscopy

Strain GFP-PTS1/WT was precultured in the YPD medium at 28°C and 180 rpm overnight, then collected by centrifugation at 10 000 $\times$ *g* for 5 min at 4°C and washed three times using sterilized ultrapure water. The cell pellets were then induced in the L-MeOH/YNB and H-MeOH/YNB media at an optical density (OD$_{660}$) of 0.5, followed by incubation at 28°C and 180 rpm for 16 h. After cultivation, the strain induced under L-MeOH or H-MeOH conditions was centrifuged at 10 000 $\times$ *g* for 5 min at 4°C. The cell pellets were diluted with sterilized ultrapure water at the concentration of OD$_{660}$ of 0.5 and immediately underwent fluorescence microscopy (OLYMPUS BX53, Olympus, Tokyo, Japan). The objective used was an oil-immersion lens (UPLSAPO 100XO, 1.4 NA, Olympus). GFP was imaged with 488 nm wavelength laser excitation and a 520 nm emission filter, and was captured by CELL F software (Olympus).

Data analysis

All experiments were repeated three times using three parallel treatments. Statistical analysis of significance between each group was carried out by Student's *t*-test using IBM SPSS Statistics 22. A *P*-value <0.05 was considered statistically significant. All data are expressed as the mean $\pm$ standard error.

Conflict of interest

The authors declare that they have no conflicts of interest.

References

Antoniewicz, M.R. (2019) Synthetic methylotrophy: strategies to assimilate methanol for growth and chemicals production. *Curr Opin Biotechnol* **59:** 165–174.

Bradford, M.M. (1976) A rapid and sensitive method for the quantitation of microgram quantities of protein utilizing the principle of protein-dye binding. *Anal Biochem* **72:** 248–254.

Chistoserdova, L. (2015) Methylotrophs in natural habitats: current insights through metagenomics. *Appl Microbiol Biotechnol* **99:** 5763–5779.

Cos, O., Ramón, R., Montesinos, J.L., and Valero, F. (2006) Operational strategies, monitoring and control of heterologous protein production in the methylotrophic yeast *Pichia pastoris* under different promoters: a review. *Microb Cell Fact* **5:** 17.

Cui, Y., Li, H., Wu, S., Zhao, R., Du, D., Ding, Y., *et al.* (2016) Formaldehyde impairs transepithelial sodium transport. *Sci Rep* **6:** 35857.

Douma, A.C., Veenhuis, M., de Koning, W., Evers, M., and Harder, W. (1985) Dihydroxyacetone synthase is localized in the peroxisomal matrix of methanol-grown *Hansenula polymorpha*. *Arch Microbiol* **143:** 237–243.

Fabarius, J.T., Wegat, V., Roth, A., and Sieber, V. (2021) Synthetic methylotrophy in yeasts: towards a circular bioeconomy. *Trends Biotechnol* **39:** 348–358.

Fei, Q., Guarnieri, M.T., Tao, L., Laurens, L.M., Dowe, N., and Pienkos, P.T. (2014) Bioconversion of natural gas to liquid fuel: opportunities and challenges. *Biotechnol Adv* **32:** 596–614.

Foyer, C.H., and Halliwell, B. (1976) The presence of glutathione and glutathione reductase in chloroplasts: a proposed role in ascorbic acid metabolism. *Planta* **133:** 21–25.

Fujimura, S., Nakagawa, T., Ito, T., Matsufuji, Y., Miyaji, T., and Tomizuka, N. (2007) Peroxisomal metabolism is regulated by an oxygen-recognition system through organelle crosstalk between the mitochondria and peroxisomes. *Yeast* **24:** 491–498.

Fukuoka, H., Kawase, T., Oku, M., Yurimoto, H., Sakai, Y., Hayakawa, T., and Nakagawa, T. (2019) Peroxisomal Fba2p and Tal2p complementally function in the rearrangement pathway for xylulose 5-phosphate in the methylotrophic yeast *Pichia pastoris*. *J Biosci Bioeng* **128:** 33–38.

Grant, C.M., Collinson, L.P., Roe, J.H., and Dawes, I.W. (1996) Yeast glutathione reductase is required for protection against oxidative stress and is a target gene for yAP-1 transcriptional regulation. *Mol Microbiol* **21:** 171–179.

Hartner, F.S., and Glieder, A. (2006) Regulation of methanol utilisation pathway genes in yeasts. *Microb Cell Fact* **5:** 39.

Hiep, T.T., Noskov, V.N., and Pavlov, Y.I. (1993) Transformation in the methylotrophic yeast *Pichia methanolica* utilizing homologous *ADE1* and heterologous *Saccharomyces cerevisiae ADE2* and *LEU2* genes as genetic markers. *Yeast* **9:** 1189–1197.

Horiguchi, H., Yurimoto, H., Kato, N., and Sakai, Y. (2001a) Antioxidant system within yeast peroxisome biochemical and physiological characterization of CbPmp20 in the methylotrophic yeast *Candida boidinii*. *J Biol Chem* **276:** 14279–14288.

Horiguchi, H., Yurimoto, H., Goh, T., Nakagawa, T., Kato, N., and Sakai, Y. (2001b) Peroxisomal catalase in the methylotrophic yeast *Candida boidinii*: transport efficiency and metabolic significance. *J Bacteriol* **183:** 6372–6383.

Ito, T., Fujimura, S., Uchino, M., Tanaka, N., Matsufuji, Y., Miyaji, T., *et al.* (2007) Distribution, diversity and regulation of alcohol oxidase isozymes, and phylogenetic relationships of methylotrophic yeasts. *Yeast* **24:** 523–532.

Ito, T., Ito, D., Ozawa, S., Fujimura, S., Matsufuji, Y., Nakagawa, J., *et al.* (2011) Molecular characterization of the *PEX14* gene from the methylotrophic yeast *Pichia methanolica*. *J Biosci Bioeng* **111:** 624–627.

Jentzsch, A.M., Bachmann, H., Fürst, P., and Biesalski, H.K. (1996) Improved analysis of malondialdehyde in human body fluids. *Free Radic Bio Med* **20:** 251–256.

Kurtzman, C.P. (2005) Description of *Komagataella phaffii* sp. nov. and the transfer of *Pichia pseudopastoris* to the methylotrophic yeast genus *Komagataella*. *Int J Syst Evol Microbiol* **55:** 973–976.

Kurtzman, C.P., and Robnett, C.J. (1998) Identification and phylogeny of ascomycetous yeasts from analysis of nuclear large-subunit (26S) ribosomal DNA partial sequences. *Antonie Van Leeuwenhoek* **73:** 331–371.

Livak, K.J., and Schmittgen, T.D. (2001) Analysis of relative gene expression data using real-time quantitative PCR and the $2^{-\Delta\Delta CT}$ method. *Methods* **25:** 402–408.

Matsufuji, Y., Yamamoto, K., Yamauchi, K., Mitsunaga, T., Hayakawa, T., and Nakagawa, T. (2013) Novel physiological roles for glutathione in sequestering acetaldehyde to confer acetaldehyde tolerance in *Saccharomyces cerevisiae*. *Appl Microbiol Biotechnol* **97:** 297–303.

Nakagawa, T., Fujimura, S., Ito, T., Matsufuji, Y., Ozawa, S., Miyaji, T., *et al.* (2010a) Molecular characterization of two genes with high similarity to the dihydroxyacetone synthase gene in the methylotrophic yeast *Pichia methanolica*. *Biosci Biotechnol Biochem* **74:** 1491–1493.

Nakagawa, T., Inagaki, A., Ito, T., Fujimura, S., Miyaji, T., Yurimoto, H., *et al.* (2006) Regulation of two distinct alcohol oxidase promoters in the methylotrophic yeast *Pichia methanolica*. *Yeast* **23:** 15–22.

Nakagawa, T., Ito, T., Fujimura, S., Chikui, M., Mizumura, T., Miyaji, T., *et al.* (2004) Molecular characterization of the glutathione-dependent formaldehyde dehydrogenase gene *FLD1* from the methylotrophic yeast *Pichia methanolica*. *Yeast* **21:** 445–453.

Nakagawa, T., Mizumura, T., Mukaiyama, H., Miyaji, T., Yurimoto, H., Kato, N., *et al.* (2002) Physiological role of the second alcohol oxidase gene *MOD2* in the methylotrophic growth of *Pichia methanolica*. *Yeast* **19:** 1067–1073.

Nakagawa, T., Mukaiyama, H., Yurimoto, H., Sakai, Y., and Kato, N. (1999) Alcohol oxidase hybrid oligomers formed *in vivo* and *in vitro*. *Yeast* **15:** 1223–1230.

Nakagawa, T., Sakai, Y., Mukaiyama, H., Mizumura, T., Miyaji, T., Yurimoto, H., *et al.* (2001) Analysis of alcohol oxidase isozymes in gene-disrupted strains of methylotrophic yeast *Pichia methanolica*. *J Biosci Bioeng* **91:** 225–227.

Nakagawa, T., Uchimura, T., and Komagata, K. (1996) Isozymes of methanol oxidase in a methanol-utilizing yeast, *Pichia methanolica* IAM 12901. *J Ferment Bioeng* **81:** 498–503.

Nakagawa, T., Wakayama, K., and Hayakawa, T. (2015) Selection of suitably non-repressing carbon sources for expression of alcohol oxidase isozyme promoters in the

methylotrophic yeast *Pichia methanolica. J Biosci Bioeng* **120:** 41–44.

Nakagawa, T., Yoshida, K., Takeuchi, A., Ito, T., Fujimura, S., Matsufuji, Y., *et al.* (2010b) The peroxisomal catalase gene in the methylotrophic yeast *Pichia methanolica. Biosci Biotechnol Biochem* **74:** 1733–1735.

Ohashi, Y., Hirayama, A., Ishikawa, T., Nakamura, S., Shimizu, K., Ueno, Y., *et al.* (2008) Depiction of metabolome changes in histidine-starved *Escherichia coli* by CE-TOFMS. *Mol Biosyst* **4:** 135–147.

Ooga, T., Sato, H., Nagashima, A., Sasaki, K., Tomita, M., Soga, T., and Ohashi, Y. (2011) Metabolomic anatomy of an animal model revealing homeostatic imbalances in dyslipidaemia. *Mol Biosyst* **7:** 1217–1223.

Palma, M., Guerreiro, J.F., and Sá-Correia, I. (2018) Adaptive response and tolerance to acetic acid in *Saccharomyces cerevisiae* and *Zygosaccharomyces bailii*: a physiological genomics perspective. *Front Microbiol* **9:** 274.

Patiño, M.A., Ortiz, J.P., Velásquez, M., and Stambuk, B.U. (2019) D-Xylose consumption by nonrecombinant *Saccharomyces cerevisiae*: a review. *Yeast* **36:** 541–556.

Porro, D., Sauer, M., Branduardi, P., and Mattanovich, D. (2005) Recombinant protein production in yeasts. *Mol Biotechnol* **31:** 245–259.

Pryor, W.A. (1991) The antioxidant nutrients and disease prevention-what do we know and what do we need to find out? *Am J Clin Nutr* **53:** 391–393.

Raymond, C.K., Bukowski, T., Holderman, S.D., Ching, A.F., Vanaja, E., and Stamm, M.R. (1998) Development of the methylotrophic yeast *Pichia methanolica* for the expression of the 65 kilodalton isoform of human glutamate decarboxylase. *Yeast* **14:** 11–23.

Royall, J.A., and Ischiropoulos, H. (1993) Evaluation of 2′,7′-dichlorofluorescin and dihydrorhodamine 123 as fluorescent probes for intracellular H_2O_2 in cultured endothelial cells. *Arch Biochem Biophys* **302:** 348–355.

Rubattu, S., Pagliaro, B., Pierelli, G., Santolamazza, C., Castro, S.D., Mennuni, S., and Volpe, M. (2014) Pathogenesis of target organ damage in hypertension: role of mitochondrial oxidative stress. *Int J Mol Sci* **16:** 823–839.

Rußmayer, H., Buchetics, M., Gruber, C., Valli, M., Grillitsch, K., Modarres, G., *et al.* (2015) Systems-level organization of yeast methylotrophic lifestyle. *BMC Biol* **13:** 80.

Sakai, Y., Nakagawa, T., Shimase, M., and Kato, N. (1998) Regulation and physiological role of the *DAS1* gene, encoding dihydroxyacetone synthase, in the methylotrophic yeast *Candida boidinii. J Bacteriol* **180:** 5885–5890.

Sugimoto, M., Goto, H., Otomo, K., Ito, M., Onuma, H., Suzuki, A., *et al.* (2010) Metabolomic profiles and sensory attributes of edamame under various storage duration and temperature conditions. *J Agric Food Chem* **58:** 8418–8425.

Tan, J., Abdel-Rahman, M.A., and Sonomoto, K. (2018) Biorefinery-based lactic acid fermentation: microbial

production of pure monomer product. *Adv Polym Sci* **279:** 27–66.

Tsuchiya, M., Suematsu, M., and Suzuki, H. (1994) *In vivo* visualization of oxygen radical-dependent photoemission. *Methods Enzymol* **233:** 128–140.

Wakayama, K., Yamaguchi, S., Takeuchi, A., Mizumura, T., Ozawa, S., Tomizuka, N., *et al.* (2016) Regulation of intracellular formaldehyde toxicity during methanol metabolism of the methylotrophic yeast *Pichia methanolica. J Biosci Bioeng* **122:** 545–549.

Whitaker, W.B., Sandoval, N.R., Bennett, R.K., Fast, A.G., and Papoutsakis, E.T. (2015) Synthetic methylotrophy: engineering the production of biofuels and chemicals based on the biology of aerobic methanol utilization. *Curr Opin Biotechnol* **33:** 165–175.

Xu, C.L., and Bell, L. (2014) Global reserves, oil production show increases for 2014. *Oil Gas J* **112:** 30–31.

Yamada, Y., Maeda, K., and Mikata, K. (1994) The phylogenetic relationships of the hat-shaped ascospore-forming, nitrate-assimilating *Pichia* species, formerly classified in the genus *Hansenula* Sydow, et Sydow based on the partial sequences of 18S ribosomal and 26S ribosomal RNAs (*Saccharomycetaceae*) – The proposals of 3 new genera, *Ogataea, Kuraishia,* and *Nakazawaea. Biosci Biotechnol Biochem* **58:** 1245–1257.

Yano, T., Takigami, E., Yurimoto, H., and Sakai, Y. (2009) Yap1-regulated glutathione redox system curtails accumulation of formaldehyde and reactive oxygen species in methanol metabolism of *Pichia pastoris. Eukaryot Cell* **8:** 540–549.

Yurimoto, H., Oku, M., and Sakai, Y. (2011) Yeast methylotrophy: metabolism, gene regulation and peroxisome homeostasis. *Int J Microbiol* **2011:** 101298.

Zhang, M., Yuan, X.J., Zhang, C., Zhu, L.P., Mo, X.H., Chen, W.J., *et al.* (2019) Bioconversion of methanol into value-added chemicals in native and synthetic methylotrophs. *Curr issues Mol biol* **33:** 225–236.

Supporting information

Additional supporting information may be found online in the Supporting Information section at the end of the article.

Fig S1. Morphology of peroxisomes in the L-MeOH and H-MeOH-grown cells using strain GFP-PTS1/WT. L-MeOH, 1% (low) methanol; H-MeOH, 5% (high) methanol.

Table S1. Detected metabolites in the Glc, L-MeOH and H-MeOH grown cells analyzed by CE-TOFMS.

Table S2. Quantification of the target metabolites in the Glc, L-MeOH and H-MeOH grown cells detected by CE-TOFMS.

Table S3. The clustering results by HCA.

Table S4. Oigonucleotide primers used in this study.